
Article:
Chappell, HF orcid.org/0000-0003-2043-0422, Jugdaohsingh, R and Powell, JJ (2020) Physiological silicon incorporation into bone mineral requires orthosilicic acid metabolism to SiO_4^{4-}. Journal of the Royal Society Interface, 17 (167). 20200145. ISSN 1742-5662

https://doi.org/10.1098/rsif.2020.0145

Physiological Silicon Incorporation into Bone Mineral Requires Orthosilicic Acid Metabolism to SiO_4^{4-}

Helen F. Chappell[1*], Ravin Jugdaohsingh[2] and Jonathan J. Powell[2]

[1]School of Food Science & Nutrition, University of Leeds,
Woodhouse Lane, Leeds, LS2 9JT
[2] Biomineral Research Group, Department of Veterinary Medicine, University of Cambridge, Madingley Road, Cambridge CB3 0ES, UK.

[*]h.f.chappell@leeds.ac.uk

Abstract

Under physiological conditions, the predominant form of bioavailable silicon is orthosilicic acid (OSA). In this study, given silicon's recognized positive effect on bone growth and integrity, we examined the chemical form and position of this natural silicon source in the inorganic bone mineral hydroxyapatite (HA). X-ray diffraction of rat tibia bone mineral showed that the mineral phase was similar to that of phase-pure hydroxyapatite. However, theoretical XRD patterns revealed that at the levels found in bone, the 'Si effect' would be virtually undetectable. Thus we used First Principles Density Functional Theory (DFT) calculations to explore the energetic and geometric consequences of substituting OSA into a large HA model. Formation energy analysis revealed that OSA is not favourable as a neutral interstitial substitution but can be incorporated as a silicate ion substituting for a phosphate ion suggesting that incorporation will only occur under specific conditions at the bone-remodelling interface and that dietary forms of Si will be metabolized to simpler chemical forms, specifically SiO_4^{4-}. Furthermore, we show that this substitution, at the low silicate concentrations found in the biological environment, is likely to be a driver of calcium phosphate crystallization from an amorphous to a fully mineralized state.

Keywords

Silicon; bone structure; mineralisation drivers; orthosilicic acid

Introduction

Dietary silicon (Si) intake, estimated at 20-50 mg ingested/person/day in the western world[1,2], largely comes in the form of digestible phytolytic silica from plants (primarily cereals) and as orthosilicic acid (OSA), a weak acid with a pKa of 9.8[3], in fluids such as drinking water. Various studies have shown that it is the soluble OSA component, either from direct ingestion or following digestion in the gut, that is readily absorbed, rapidly increasing serum Si levels[4,5].

The impact of this dietary Si appears to be a positive effect on connective tissue growth and maintenance. The earliest studies of Carlisle and Schwarz showed dramatic detrimental changes in the structure of bone and collagenous tissues, such as skull deformities in rats and absent wattles and combs in chicks, when dietary Si deprivation was induced[6,7]. Subsequent work, which has frequently been hampered by the difficulty in achieving truly Si-free diets, has shown smaller, but significant changes in bone structure such as a reduction in both the phosphate content of bone and the tibia growth plate thickness in Si-deprived animals[8]. Whilst the precise role of Si in bone tissue has yet to be determined, there are a number of important observations that have been made. For example, a relatively recent study showed that bone retains its silicon content even with imposed dietary deprivation[8]; rats, stressed in this way, shut down Si excretion in urine and appear to conserve their already acquired Si for connective tissue function[8], whilst still displaying a relatively normal phenotype. Recently identified mammalian Si transporters may enable this Si conservation[9, 10]. Furthermore, in contrast to bone *collagen* Si levels, which have been shown to be constant regardless of *total* bone Si-levels[11], Jugdaohsingh *et al* revealed that bone *mineral* can vary quite markedly, by about an order of magnitude, in its Si content[11]. The implications of this are not yet clear although it is understood that (a) men, post-menopausal women taking Hormone Replacement Therapy (HRT) and pre-menopausal women, show a positive relationship between dietary Si intakes and bone mineral density[12,13] and (b) when growing rats were supplemented with a highly bioavailable form of dietary Si (namely monomethylsilanetriol, MMST) their increase in Si status, adjudged from fasting serum Si levels, positively correlated with their increase in bone mineral density (BMD)[14].

It is unsurprising therefore that Si is now an integral part of regenerative bone materials. The very first Si-containing bioactive material was Hench's resorbable Bioglass, namely 45S5[15,16,17], although it was the Ca:P ratio that was considered important in driving bone apposition and bonding, rather than the inclusion of the silica

matrix. Subsequently, however, as the potential of silicon as a biologically advantageous agent was explored, Si-substituted calcium phosphate cements and coatings were specifically developed. Indeed, Si substitution has been used very effectively in commercially available calcium phosphate bone-graft materials for some years[18,19,20,21]. It has been shown to increase the rate of bone ingrowth[22], and promote the remodelling of bone at the material-bone interface[23]. Additionally, Si-substituted hydroxyapatite (HA) supports and improves the attachment and proliferation of mesenchymal stem cells and induces osteogenesis to a greater extent than the phase-pure material[24,25]. It is also worth noting that computational studies have played a particularly significant role in examining the effects and consequences of a number of ion substitutions, including those involving Si, on potential bone-graft materials, both in bulk and surface aqueous environments[26,27,28,29,30]. An especially useful review is provided by de Leeuw[31].

However, it has been suggested, through a combination of experimental analysis and thermodynamic modelling that the most likely chemical form of Si in mineral-based biomaterials is SiO_4 and not the neutral OSA molecule that is found in the diet[23,32,33,34]. Analysis by Fourier Transform Infrared Spectroscopy (FTIR), in particular, has revealed a decrease in both the hydroxyl and phosphate stretching bands, which has been interpreted as the substitution of phosphate tetrahedra by silicate tetrahedra and the concomitant loss of hydroxyl ions[25,35,] a mechanism first proposed by Gibson et al[36]. Thermodynamically, this mechanism has also been shown to be valid by first principles simulations[32,33]. However, due to the combined effects of low Si substitution levels in bone mineral and the insensitivity of ^{29}Si Nuclear Magnetic Resonance (NMR), it has been impossible to unanimously resolve the chemical speciation of physiological silicon; indeed this is difficult in synthetic minerals despite their much higher Si-substitution levels[35, 37, 38], and it is rarely demonstrated. The nature of the silicon anion in calcium phosphates was recently addressed by Duncan et al who performed solid state ^{29}Si NMR on silicon-substituted tricalcium phosphate. Interestingly, this study revealed silicon Q^0 (SiO_4^{4-}) and Q^1/Q^2 species within the crystal structure. These polymerized, disilicate ions (Q^1/Q^2), suggest larger silicate species within the structure, which perhaps indicate an alternative charge compensation mechanism that doesn't involve the loss of hydroxyl ions, but rather, loss of oxygen[39]. Other silicate anions, in particular SiO_3OH have been detected in several other silicate minerals including afwillite and a number of uranyl silicates[40]. In afwillite, the decrease in symmetry of the silicate tetrahedron caused by the single protonation is reflected in changing Raman stretching and bending vibrations.

108 It is notable that these bands fall in the same range as those frequently observed in Si-
109 substituted HA[39,40].
110
111 By contrast, in numerous studies on the effects of Si in animal models, OSA and its pro-
112 forms are the most frequently employed dietary Si sources, due to OSA's bioavailability
113 and ready absorption[4,8,41]. OSA is a weak acid (pKa 9.8) and it has long been assumed by
114 biologists and physiologists that it remains fully protonated and charge-neutral
115 throughout its physiological pathways. Indeed, in silica-mineralizing species such as the
116 choanoflagellates, silicic acid is known to be the predominant precursor to silica
117 extrusion[42]. Notwithstanding, a recent study on silicic acid transporters in eukaryotic
118 algae suggests that physiological deprotonation *can* occur, and that OSA is transported
119 across the cell membrane through the single ionization of OSA to $Si(OH)_3O^-$, mediated
120 through a close interaction with a sodium ion in the transporter binding pocket[43].
121 Nevertheless, currently, there is no known driving force for consecutive deprotonation
122 in mammals that would resolve the chemical inconsistency between synthetic
123 biomaterials, where synthesis conditions drive deprotonation of silicate, and
124 mammalian physiology, where physiological conditions alone would suggest OSA
125 remains fully protonated. Therefore we now ask the question, can OSA, as a neutral
126 molecule, find its way into bone mineral in a thermodynamically favourable manner
127 without the need of a *physiological* deprotonation mechanism? Additionally, we explore
128 the energetic cost of including increasing concentrations of silicon in the structure of
129 precursor calcium phosphate clusters to determine if these particles, whatever their
130 formation mechanism, would be thermodynamically stable. It is also worth noting that
131 there are other organic molecules, such as citrate, that have already been shown to be
132 integral to the mineral phase of bone, suggesting that size considerations alone are not
133 enough to eliminate the potential for OSA inclusion[44].
134
135 **Materials & Methods**
136
137 ***Computational Methods***
138 *Crystalline HA Model*
139 A model of HA (previously described[30]) was employed as a proxy for the bone mineral
140 structure. The exact composition of bone mineral is still widely debated, but analyses of
141 bone tissue consistently show that HA-like mineral can be readily identified as the major
142 mineral component[45]. It should be noted, however, that phase-pure HA represents a
143 simplification of natural bone mineral, which is subject to ion substitutions, principally

144 carbonate and non-Ca cations[46]. As bone mineral is a well-established sink for cations,
145 the composition of biological HA varies quite significantly between people of different
146 ages, sexes, occupation and location[47]. For this reason, we have chosen the least
147 complicated approximation to bone mineral, namely phase-pure HA, which has
148 previously been successfully employed for comparison with, and elucidation of,
149 experimental data[33, 48]. Briefly, the basic HA structure consists of a hexagonal unit cell
150 composed of 44 atoms and space group $P6_3/m$. To prevent interactions of periodic
151 images through the periodic boundary conditions, substitutions were made into a 4-unit
152 cell model (1x2x2), composed of 176 atoms. Hydroxyl ions were ordered along the *c*-
153 axis in OH-OH chains, which has been shown to be the most energetically favourable
154 arrangement[49, 50]. Within our model, which has a number of *c*-axis channels, it would
155 have been possible to create alternate domains of all up-facing and all downward-facing
156 hydroxyl ions, this arrangement having been shown to have a slight energetic
157 advantage[50]. However, these alternating domains, which have been used to explain the
158 observed disorder in the OH positions, have also been shown, experimentally[51], to form
159 a monoclinic, rather than hexagonal, crystal. Therefore, in this work we decided to leave
160 the hydroxyl ions in alternate channels orientated in the same direction but allowed
161 them complete freedom to move. Unconstraining the hydroxyl ions in this way also
162 accounts for the previously observed disorder, due to the rotation of the ions[33].
163 Geometry optimization of the phase-pure 4-unit cell HA model, followed by OSA
164 and Si substitutions, were carried out using the plane-wave Density Functional Theory
165 (DFT) code, CASTEP[52]. As it is well established that biological apatite has more disorder,
166 or amorphous characteristics than synthesized phase-pure mineral, the symmetry of the
167 cell was transformed to *P1*, allowing all lattice parameters and atomic positions
168 complete freedom in all planes. Convergence testing assigned a kinetic energy cut-off of
169 430 eV for all calculations. Sampling of the Brillouin zone was carried out with a 4×3×3
170 *k*-point grid[53]. Ultrasoft pseudopotentials (BIOVIA library) were employed[54] along with
171 the generalized gradient approximation (GGA) and PBE exchange-correlation
172 functional[55]. Convergence tolerances for energy change, maximum displacement,
173 maximum force and maximum stress were set at 1×10^{-5} eV atom^{-1}, 0.001 Å, 0.03 eV Å^{-1}
174 and 0.05 GPa respectively.
175 The OSA molecule (Figure 1a) was positioned within the HA model (Figure 1b)
176 either as a neutral interstitial molecule or as a substitution for a phosphate ion. The
177 interstitial molecule was initially positioned to maximize the distance from all other ions
178 (Figure 2). It should be noted, however, that other positions within the model could,
179 potentially, have been used as a starting configuration and the optimized geometry is

therefore only one of a range of possibilities. However, as all phosphate ion positions are equivalent and there are only two different crystallographic calcium sites[56], the environment for any interstitial position would be similar.

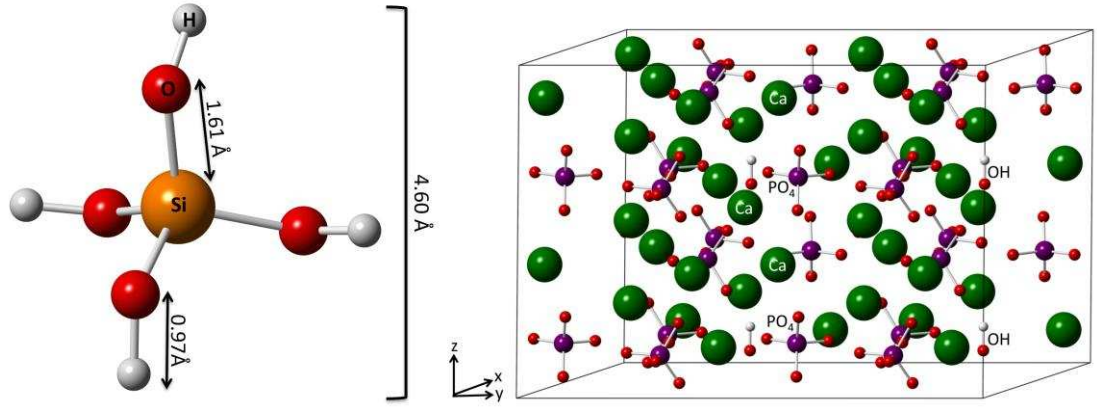

(a) **(b)**

Figure 1. (a) Optimized structure of OSA. **(b)** Optimized HA model, showing the three principle axes. The figure shows silicon in orange (a), oxygen in red, hydrogen in white, calcium in green and phosphorus in purple.

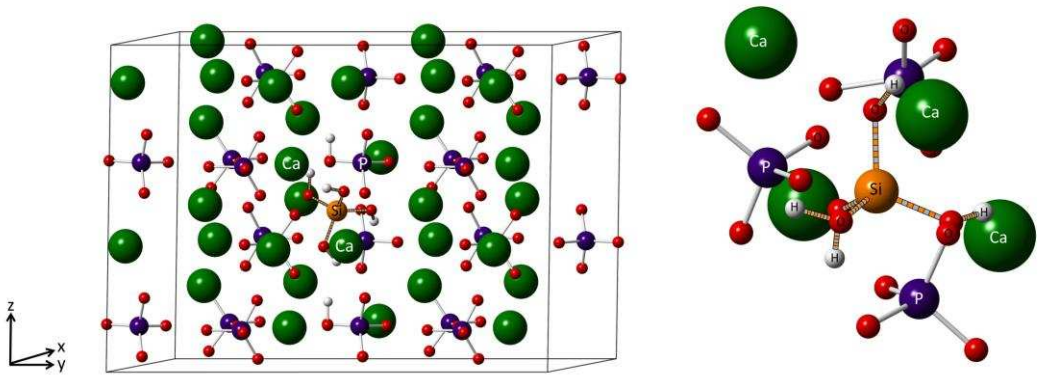

(a) **(b)**

Figure 2. (a) Interstitial OSA shown in its starting position within the HA model. **(b)** A close-up view of the interstitial OSA molecule in its starting position. Silicon is shown in orange, oxygen in red, hydrogen in white, calcium in green and phosphorus in purple. Bonds within the OSA molecule are shown banded in grey and orange.

In addition to a neutral OSA interstitial substitution, alternate substitutions were made with chemically modified forms of OSA. Firstly, a PO_4 ion was replaced with a SiO_4 ion and concomitant OH ion removal. This substitution is familiar within the context of

biomaterials production, and has been shown to occur at time of synthesis or during sintering[33]. Additionally, OSA was substituted in a singly protonated form, namely SiO_3OH, for a PO_4 ion. This latter substitution, which has been observed as an anion in other silicate minerals[40], allows for the substitution without the need for other charge compensatory ion removal (i.e. no OH ions need be removed). A previous computational study that looked at the two PO_4 substitutions in a smaller model structure, but not the neutral OSA substitution, showed that the SiO_4 ion has much greater affinity for the excess hydrogen than the PO_4 ions[32] so here we do not again explore this alternative charge compensation possibility (i.e. PO_4H / SiO_4). Although the PO_4 substitutions have been previously calculated in smaller models, it is important for accurate comparison with the new substitution, that they are re-visited here under identical conditions.

To discriminate between the various substitutions, formation energies, which enable comparison between each substitution site configuration, were calculated. Equations (1), (2) and (3) show how the formation energies were calculated for (1) an interstitial OSA substitution, (2) SiO_3OH for PO_4 and (3) SiO_4 for PO_4 with concomitant OH removal:

$$E_f = E_{HA\_Int} \quad \left(E_{HA} + E_{OSA}\right) \quad \textbf{(1)}$$

$$E_f = E_{HA\_SiO4H} \quad \left(E_{HA} + E_{SiO4H} \quad E_{PO4}\right) \quad \textbf{(2)}$$

$$E_f = E_{HA\_Si\ OH} \quad \left(E_{HA\ OH} + \quad {}_{Si} \quad {}_{P}\right) \quad \textbf{(3)}$$

where E_{HA_Int} is the energy of the HA model substituted with an interstitial OSA molecule, E_{HA} is the energy of the phase-pure HA model, E_{OSA} is the energy of the OSA molecule, E_{HA_SiO4H} is the energy of the HA model with an SiO_3OH substitution replacing PO_4, E_{SiO4H} is the energy of an SiO_3OH molecule, E_{PO4} is the energy of a PO_4 ion, $E_{HA\_Si\text{-}OH}$ is the energy of the HA model in which SiO_4 has replaced PO_4 and an OH ion has been removed, $E_{HA\text{-}OH}$ is the energy of the HA model with OH removed, μ_{Si} is the chemical potential of silicon and μ_P is the chemical potential of phosphorus. Chemical potentials for the single element substitutions (namely Si and P, and H for the amorphous model described below) were calculated, using DFT, from the lowest energy sources, as previously described[57]. An extensive range of sources and sinks were examined, including two

polymorphs of elemental phosphorus, phosphoric oxide, quartz and cristobalite[57]. Final values, calculated at the same cut-off energy as OSA, were obtained from elemental silicon and monoclinic phosphorus. For the amorphous model, described below, the H chemical potential was determined from an isolated H_2 molecule in vacuum.

Amorphous HA Model

To examine the stability of potential particle compositions, an amorphous model was created. This model, based on Posner's cluster, was treated as an isolated molecule in a large simulation box of 20 Å x 20 Å x 20 Å. The box size was determined by energy convergence testing to ensure periodic images did not interact. The box dimensions were constrained throughout the geometry optimization while the atomic positions had freedom in all planes. To ensure comparability, optimization was carried out under the same conditions as the crystalline model, using the CASTEP[52] DFT code and a kinetic energy cut-off of 430 eV. Convergence tolerances for energy change, maximum displacement and maximum force were also set at 1×10^{-5} eV atom^{-1}, 0.001 Å and 0.03 eV Å^{-1} respectively. Substitution formation energies were calculated in the same way as those in the crystalline model,

$$E_f = E_{AmSub\_x} - (E_{Am} - x\mu_P + x\mu_{Si} + x\mu_H) \quad \textbf{(4)}$$

where E_{AmSub} is the energy of the Si-substituted amorphous model, E_{Am} is the energy of the phase-pure amorphous model, μ_P is the chemical potential of phosphorus, μ_{Si} is the chemical potential of silicon and μ_H is the chemical potential of hydrogen and x is the number of Si substitutions.

It should be noted that in order to establish substitutional stability, we have undertaken thermodynamic geometry optimization for these calculations and not dynamical simulations. Whilst dynamic simulations that include explicit water within the system would be able to elucidate particle nucleation mechanisms, the advantage of the thermodynamic simulations is their ability to directly compare the potential energetic stability of various compositions, regardless of formation kinetics. As such we are able to determine which silicate species exists in this matrix based upon first principle approaches, allowing for later work that may then determine its incorporation mechanism.

X-ray Diffraction

We present new data on bone samples reserved from previous experimental studies in rats[8,58]. Powder X-ray diffraction was undertaken on tibia samples from female Sprague Dawley rats exposed to two different diets for 26 weeks, which resulted in bones with either a low (0.97 μg Si/g bone mineral)[58] or a high (12.98 μg Si/g bone mineral)[8] Si content. The low Si content bone came from a rat fed on a standard rodent chow diet and the high Si content bone came from a rat fed on a standard rodent diet composed of wheat, barley and soya meal, wheat-feed, fish meal, fats and oils, minerals, trace elements and molasses[58]. Full details of the study design and ethical approval, which was obtained from the UK Home Office (Animals Scientific Procedures Act 1986; Scientific Procedures on Living Animals), are given in references[8, 58]. The organic component of the bone was removed as previously described[59] and confirmed through FTIR analysis. Full details of the XRD methods and sample preparation are provided in the supplementary information of reference[14]. Elemental analysis of the bone samples (Figure 2, Supplementary Information[11]) indicated that the only major difference between the two, in terms of the major and minor elements, was Si. This suggests that Si incorporation in bone is independent of any other trace element level, making co-substitution unlikely as a significant mechanism.

Theoretical XRD patterns were calculated using CrystalDiffract®[60].

All data generated or analysed during this study are included in this published article (and its Supplementary Information file).

Results & Discussion

X-ray Diffraction

Table 1 shows the lattice parameters derived from the mineral component of two rat tibia samples: one with a high Si content (12.98 μg Si/g bone mineral) and the other with a low Si content (0.97 μg Si/g bone mineral). The XRD patterns are available in Supplementary Fig. S1 and Supplementary Fig. S2 online. Si exposure for these animals came from within their diets and, as noted above, the absorbed Si is considered to be OSA[4,5].

Si content (µg Si/g bone mineral)	R_{wp} (%)	a (Å)	error (Å)	c (Å)	error (Å)	Volume (Å^3)	error (Å^3)
0.97	6.9	9.429	0.0003	6.882	0.0002	529.845	0.048
12.98	6.2	9.424	0.0002	6.882	0.0002	529.286	0.042

Table 1. Measured lattice parameters derived from XRD spectra of tibia samples from female rats that have either a low or high Si content in the bone mineral (0.97 versus 12.98 µg/g).

Clearly (Table 1), Si incorporation into the bone mineral does not affect any large changes in the crystal structure at these levels. In fact, the lattice parameters are very similar (less than 1 % difference) to those of the phase-pure HA, which we have obtained theoretically from a DFT optimized HA unit cell (Table 2).

a (Å)	b (Å)	c (Å)	Volume (Å^3)
9.477	9.477	6.851	532.873

Table 2. Calculated phase-pure HA lattice parameters, calculated using a DFT optimized HA unit cell. While bone and HA differ in detailed composition, bone XRD patterns match HA very closely and it is a good model for comparison.

Potentially, these results suggest that either the OSA is incorporated into the bone mineral structure but, overall, has little impact on the crystallographic lattice, or, alternatively, that OSA was incorporated without disruption but in a metabolized form. This explanation can only be substantiated, however, if (1) the effects of the extremely low levels of Si in the bone mineral are actually detectable within the limits of XRD and (2) the different forms of Si show distinguishable features within those XRD patterns. To assess this theoretical XRD patterns were calculated for phase-pure HA and silicon substituted HA models. Using the theoretical spectra alone enables us to isolate the effect of Si on the mineral phase spectrum without interference from other potential differences between biological samples. The two theoretical models that were created and geometry optimized consisted of: 1) a phase-pure HA model composed of 4 unit cells (176 atoms) and 2) a Si-substituted version of the same HA model. This latter model, with one SiO_4 replacing one PO_4 and the concomitant removal of an OH ion, is a familiar substitution within the biomaterials field[30]. In this case, Si accounts for 0.7 wt % of the structure, a figure that is both achievable and often found in the production of Si-

substituted calcium phosphate materials but many orders of magnitudes higher than occurs in vivo[19,22,23]. However, in the simulated XRD pattern (Figure 3) Si substitution at this level produces only minor distinguishable features compared to that of phase-pure HA, suggesting that substitution at lower levels would be indistinguishable from phase-pure HA.

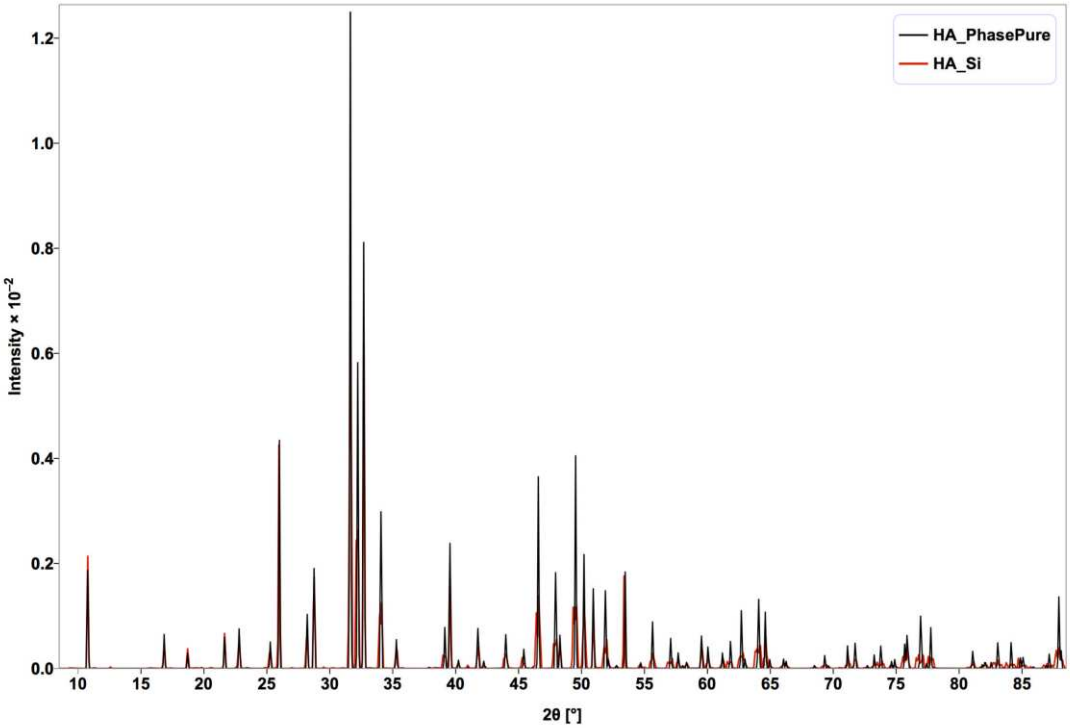

Figure 3. Simulated XRD pattern for phase-pure HA (black) and silicon substituted (0.7 wt %) HA (red).

Turning to OSA, rather than SiO_4, Figure 4a shows the simulated XRD pattern for the same HA model but with a single interstitial OSA molecule substitution; this pattern has some clearly distinguishable features compared to both the phase-pure and SiO_4 substituted HA patterns of Figure 3.

However, again, at this substitution level there is nearly 500 times as much Si per gram of mineral as in the high Si bone mineral sample of Table 1. Figure 4b therefore shows a mixed XRD pattern that blends, in the correct proportions for that high-Si sample, the phase-pure HA with the OSA interstitial pattern of Figure 4a. It is clear from this figure that at the level of substitution in our experimental samples, XRD produces a pattern that is indistinguishable from that of phase-pure HA. Consequently, we do not expect to

be able to either (a) detect Si within our experimental XRD or (b) distinguish one Si substitution site from another.

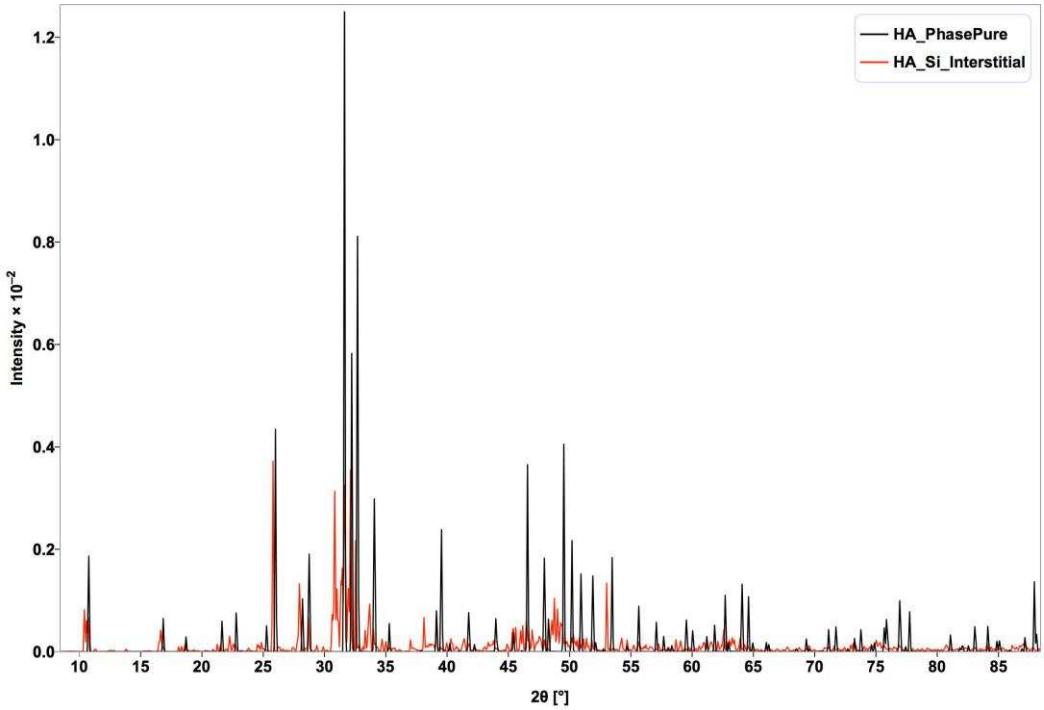

(a)

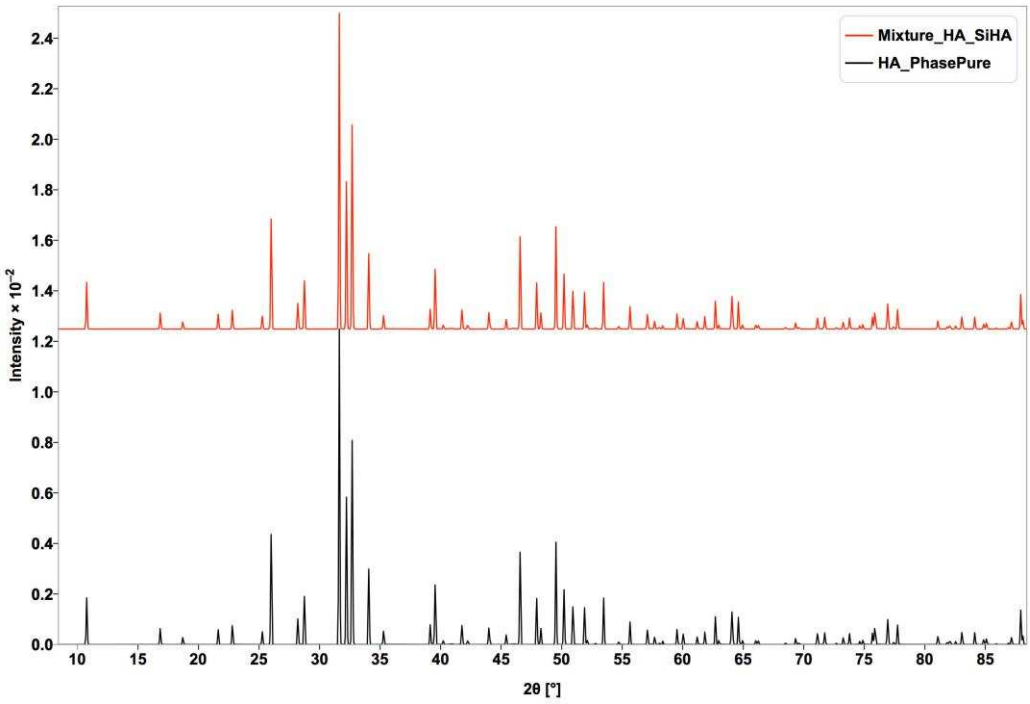

(b)

Figure 4. (a) Simulated XRD pattern for interstitial OSA in HA. (b) Stacked simulated mixed XRD pattern composed of 99.95% phase-pure HA and 0.05% interstitial OSA in HA (red, top) and, for

comparison, the phase-pure HA XRD pattern (black, lower). In terms of Si composition this is equivalent to the 'high' Si level (12.98 µg /g bone mineral) bone sample in Table 1.

Experimental methods, in particular NMR, have been used by others to try to address the speciation of Si in materials, particularly in the field of calcium phosphate biomaterials[37, 38]. However, J-coupling in solid state NMR is extremely difficult to achieve in any but the most crystalline of samples, and our own experiments (data not presented) showed no difference between bone samples of differing Si content, using ^{31}P NMR. Previously, Duncan et al, using ^{29}Si MAS NMR, established that there is an increasing disorder in the mineral phase of synthetic calcium phosphates with increasing Si-substitution levels and that, potentially, a range of (as yet unresolved) silicate species may exist in these materials[37]. ^{31}P NMR has, in addition, indicated OH ion interactions with the silicate species in similar synthetic samples[38]. However, the minute levels of Si in natural bone samples and the relative lack of crystallinity in the mineral phase, have so far precluded any analytical insights into the immediate Si environment in biological samples. Therefore, to overcome these limitations with both the XRD and NMR experimental data, we employed first principles modelling to investigate the thermodynamic favourability of different OSA substitution sites.

Formation Energy Analysis

Formation energies, which determine the thermodynamic stability of a particular crystallographic configuration, are presented in Table 3 for the three Si substitutions (as outlined in Materials & Methods) in the crystalline model.

Row	**Substitution**	**Formation Energy, E_f (eV)**
a	OSA interstitial	+6.591
b	SiO_4 for PO_4 with OH ion removal	-1.945
c	SiO_3OH for PO_4	+1.415

Table 3. Calculated formation energies of Si substitutions into the HA model.

It is clear that substituting neutral OSA into the HA unit cell as an interstitial substitution is highly unfavourable. The positive formation energy is large and suggests that chemical modification would almost certainly be required for Si to enter the mineral phase. However, still unfavourable but to a lesser extent, is substitution with the modified form of OSA, SiO_3OH. As reported previously[18], the straight substitution of SiO_4

(effectively a metabolized form of OSA) into a PO_4 site with concomitant hydroxyl removal, is a favourable substitution with a negative formation energy. A previous theoretical study that considered both the PO_4 substitutions (in a smaller model) but not the neutral OSA substitution, agrees with the results here, with the most favourable substitution being that which requires OH loss for charge compensation[32]. Additionally, the authors showed, as reported here, that with the SiO_3OH substitution, the hydrogen had a high affinity for Si; even when starting with a protonated form of PO_4 the hydrogen always transferred, under optimization, to the silicate ion[32].

	Phase-pure HA	**OSA Interstitial**	**SiO_3OH**	**SiO_4, OH removal**
***a* (Å)**	9.479	9.514 (+0.37%)	9.491 (0.12%)	9.470 (-0.09%)
***b* (Å)**	18.958	19.340 (+1.97%)	18.995 (+0.19%)	18.942 (-0.09%)
***c* (Å)**	13.697	13.803 (+0.77%)	13.715 (+0.13%)	13.719 (+0.16%)
Volume ($Å^3$)	2131.560	2229.373 (+4.39%)	2139.170 (+0.36%)	2133.529 (+0.09%)

Table 4. Calculated lattice parameters for OSA substitutions in phase-pure HA. The value in brackets shows the difference from the optimized HA values shown in the first column.

Substitution of OSA in the interstitial position causes structural disruption to the HA model, with an increase in cell volume of 4.39 %. Whilst the changes for the SiO_3OH substitution are small, they are still larger than the changes affected by the SiO_4 substitution. In this latter case the volume change is less than 0.1 %. Given that our analytical measurements (Table 1) on SiHA depart from the phase-pure HA in lattice parameters by less than 1 %, the incorporation of SiO_4 as a substitution for PO_4 is entirely plausible. Taken together with the formation energy analysis above it is entirely reasonable to conclude that the SiO4/-OH substitution is the most likely substitution in biological tissue, as often assumed of synthetic biomaterials, and that the substitution of neutral OSA can be effectively ruled out. Indeed, this convergence of opinion from both analytical methodology in prior work, and first principles theory in this study, makes for a compelling case. It should be noted however that while the SiO_3OH anion, which is found in other silicate minerals[40], is unlikely to occur, or, to occur in much smaller

427 amounts, due to the positive formation energy, the calculations here show that it can't
428 be absolutely ruled out on the lattice parameters alone.
429
430 However, the mechanism by which this favourable SiO_4 substitution is achieved when
431 dietary Si is delivered (absorbed) in the form of OSA, remains unclear, but is likely to be
432 linked with the bone remodelling process, where new mineral is laid down. Certainly, a
433 small number of studies have corroborated the original Carlisle findings that Si is
434 located within the poorly mineralized, non-calcified regions, whilst the concentrations
435 detected in fully mineralized tissue are extremely low[11,61,62,63]. These results suggest that
436 there is a role for Si during the early stages of bone formation. Recently, Jugdaohsingh *et*
437 *al*[58] also reported the marked correlation between bone collagen turnover and fasting
438 serum Si levels (a proxy for Si status) in a mammalian model, again linking Si-bone
439 interactions to the remodelling process.
440
441 *Role of Silicon*
442
443 We have shown that SiO_4 substitution for PO_4 is the only favourable substitution studied
444 here (Table 4). As such, the potential role of SiO_4 in bone mineralization was further
445 explored.
446 As noted above, Si has been detected, in very low concentrations, within the
447 immature bone areas undergoing active calcification[61,62,63]. To investigate this, an
448 amorphous model based around the bone mineral precursor known as Posner's
449 Cluster[56], was created. The purpose of these models was to assess the stability of
450 different compositions that may or may not form at the interfacial layer of
451 crystallization. To do this, a silicon-free cluster was created and substitution by silicon
452 was carried out to assess the thermodynamic stability of these compositional changes.
453 This gives a quantitative measure of the most likely compositions to form, but it does
454 not provide a mechanism for their nucleation from solution. This method has previously
455 been used successfully to understand the thermodynamics of growing silica particles in
456 the exoskeleton formation of choanoflagellates[42]. This model cluster consists of six PO_4
457 ions, as in fully crystalline HA, but accommodates only 9 calcium ions and no OH ions.
458 Consequently, the SiO_4/-OH substitution is unavailable within the cluster model.
459 Therefore, silicon substitution, in the form of SiO_3OH (for charge compensation the
460 silicate ion was singly protonated), was carried out to compare the thermodynamic
461 favourability of silicon substitution in amorphous and crystalline calcium phosphate.

Figure 5 shows the phase-pure amorphous structure and the optimized, singly silicate-substituted structure.

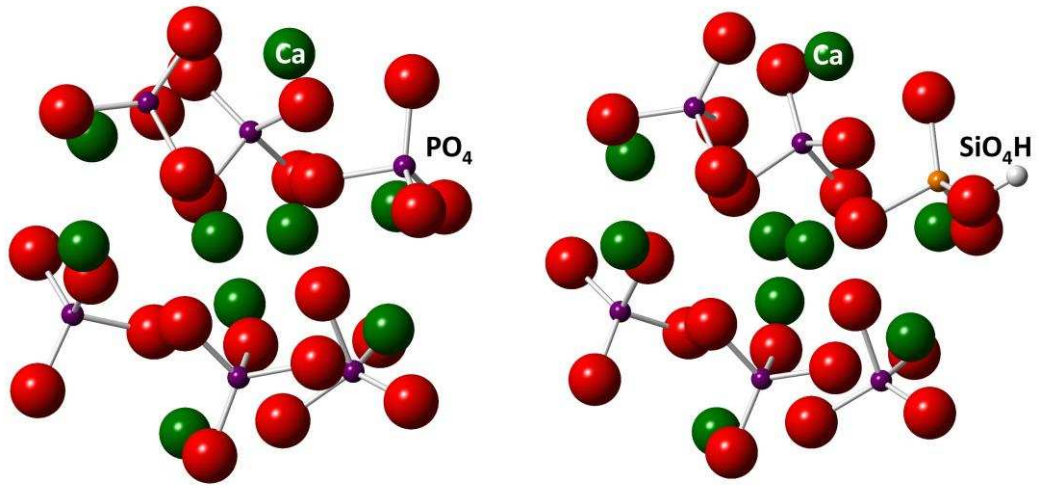

(a) **(b)**

Figure 5. (a) An optimized amorphous Posner's Cluster. **(b)** Optimized SiO_3OH substituted Posner's Cluster. Silicon is shown in orange, oxygen in red, phosphorus in purple, calcium in green and hydrogen in white.

As in the crystalline structure[32], it is the silicate ion that retains the hydrogen on optimization. The formation energies of successive silicate substitutions, taking the composition across the entire solid state series from $Ca_9(PO_4)_5(SiO_3OH)$ to $Ca_9(SiO_3OH)_6$, are presented in Table 5, along with the formation energy of the silicate substitution in phase-pure HA.

Row	Substituted Model	Formation Energy (eV)
HA_SiO4	$Ca_{10}(PO_4)_5SiO_4OH$	-1.945
1	$Ca_9(PO_4)_5(SiO_3OH)$	-0.750
2	$Ca_9(PO_4)_4(SiO_3OH)_2$	-1.520
3	$Ca_9(PO_4)_3(SiO_3OH)_3$	-1.705
4	$Ca_9(PO_4)_2(SiO_3OH)_4$	-3.835
5	$Ca_9PO_4(SiO_3OH)_5$	-2.881
6	$Ca_9(SiO_3OH)_6$	-4.140

Table 5. Calculated formation energies of increasing silicate substitution number into the amorphous calcium phosphate model. The HA_SiO_4 substitution is the substitution of SiO_4 into

phase-pure HA with concomitant OH loss. Rows **1-6** show increasing silicate substitution into the amorphous model.

These results show that silicate substitution in the amorphous calcium phosphate structure is a favourable substitution and one without apparent limit. That is, replacing successive phosphate ions with silicate ions produces increasingly stable compositions with the series end member, $Ca_9(SiO_3OH)_6$, being the most favourable and thermodynamically stable of them all. However, in mammalian samples Si is only detected at very low levels, even at the growth front of bones. Consequently, although the higher Si compositions are, in principle, favourable, there is no evidence that they would ever exist biologically.

In the current model, it is interesting to observe that up to $Ca_9(PO_4)_3(SiO_3OH)_3$, where there are equal amounts of silicate and phosphate, substitution into the fully crystalline HA model has the lower formation energy and is consequently *more* favourable than silicate being incorporated into an amorphous calcium phosphate phase. This thermodynamic cap may go some way to limiting the silicate levels in the amorphous material. Equally, it is therefore plausible that low silicate levels in amorphous young bone mineral or within the aqueous layer at the remodelling interface, may actually act as a driver of HA crystallization to satisfy the system's tendency to occupy its thermodynamically lowest energy state (i.e. crystalline HA). By this hypothesis, therefore, delivery of Si to this interface through Si-laden biomaterials may alone account for the increased rate of bone deposition, without there being any particular structural role at all for Si in the tissue. However, as already outlined above, Si-levels in the fully crystalline bone tissue are considerably lower than at the bone-remodelling front[61], so while the presence of silicate may drive the system towards crystallization, silicate does not appear to be incorporated into the biomineral to any large extent. This suggests that another mechanism, which promotes phosphate substitution for SiO_4, may exist as the maturation of the crystal progresses and may be linked to multiple components of the interfacial layer, such as small organic molecules or ions, many of which currently remain unknown or unexamined (Figure 6). Equally, migration of Si with the bone-remodelling front may concentrate Si in the interfacial layer and thus account for the observed low levels in the mature crystal; if this were the case it may suggest that in addition to driving crystallisation from the amorphous to the crystalline state, Si plays a role in signalling that has yet to be identified.

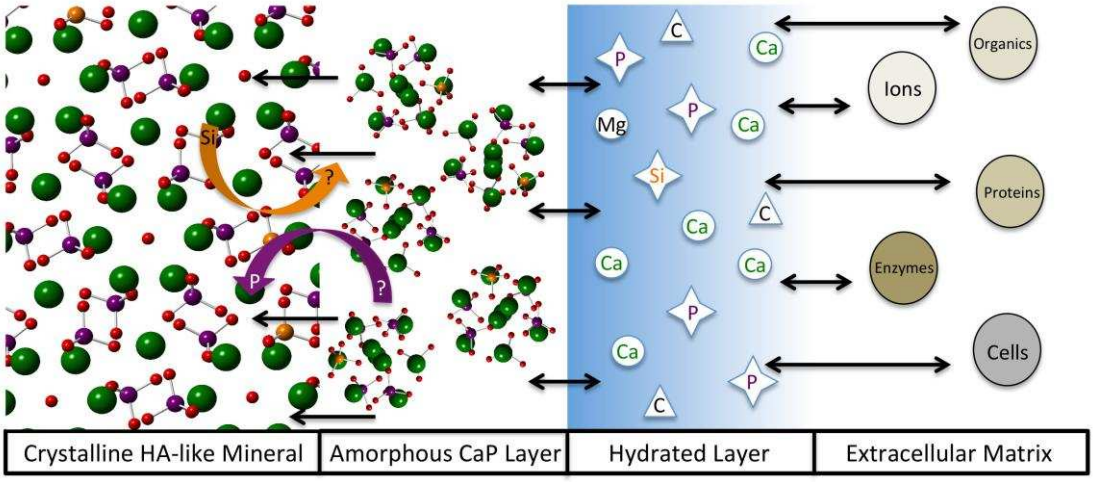

Figure 6. A simplified illustration of the mechanism of biomineralization. It is still unclear why so little Si is incorporated into mature bone mineral, when it appears to have a critical role in its formation. In the ball and stick illustrations, silicon is shown in orange, calcium in green, oxygen in red, phosphorus in purple and hydrogen in white.

Conclusions

It can be reasonably concluded from the above results that OSA would not be able to concentrate in the inorganic mineral phase of bone to any large extent in either its chemically intact or simple charge-modified forms. Specifically, further chemical modification, to SiO_4^{4-}, is required in order to maintain both energetic and geometric integrity and alleviate the large stresses and strains placed upon the crystal structure by intact molecular substitutions. Although it is possible that OSA exists in the aqueous interfacial layer during bone remodelling, our data show that the OSA in Si-containing mineral has almost certainly undergone metabolism. Previous studies have shown that in the early phases of bone remodelling, the pH of the extracellular fluid is more acidic than normal and then, as mineral is deposited, becomes more alkaline[64]. Indeed, it has been shown that the response of the osteoblasts is very sensitive to pH[65], but it should be remembered that the actual pH range across the whole remodelling process is 7.0-7.6[64,65]. Therefore, while in general the silicate may be expected to be less protonated in the more alkaline mineral deposition phase of remodelling, pH alone cannot account for a fully deprotonated silicate ion as this would require a significantly more basic environment. While it is difficult to precisely determine the isoelectric point for OSA due to the large difference between the pKa and pKb, it is usually quoted as being around 3[66]. The material point being that at any pH from ~ 3.5 to ~8.5, OSA will exist in its neutral form of $Si(OH)_4$.

Furthermore, the substitution of silicate into an amorphous model indicates that, in vacuum at least, and at low levels, silicate may be driving crystallization in order to move the system into its lowest energy – crystalline - state. This may partly explain the role of Si in bone mineralization and the reason why relatively high concentrations of Si have been detected at the bone growth front rather than in fully mineralized tissue. It may also clarify the advantageous use of Si in biomaterials, where the material essentially acts as a Si-delivery system to developing tissue. However, with adult BMD corresponding to elderly osteoporosis risk and the positive association between higher intakes of Si and increased BMD[11,12,67], further research exploring the precise role of Si in bone tissue and the mechanism by which consecutive deprotonation of OSA occurs, is clearly of great importance. Our data clearly explain the paradox that, on the one hand $Si(OH)_4$ appears to be a beneficial nutrient to bone but on the other hand it is very unreactive. The answer is that it must be metabolized to SiO_4^{4-}.

Author Contributions

All experimental work on the rat bone samples was undertaken by R. J and all computational modelling was undertaken by H. C, with discussions between the authors as to objectives and interpretation of results. The manuscript was written by H. C with contributions and editing from R. J and J. P. All authors reviewed the final manuscript.

Acknowledgements

The modelling work was performed using the Darwin Supercomputer of the University of Cambridge High Performance Computing Service (http://www.hpc.cam.ac.uk/), provided by Dell Inc. using Strategic Research Infrastructure Funding from the Higher Education Funding Council for England and funding from the Science and Technology Facilities Council. Thanks to Dr Andrew Brown & Dr Tim Comyn, University of Leeds, for conducting the XRD studies on our rat tibia bone samples and to Professor Stephen Kinrade (Lakehead University, Canada), Dr David Shepherd (De Monteforte University) and Professor Sharon Ashbrook (St Andrews University) for academic discussions.

577 **Data Accessibility**

578

579 All raw data, both X-ray diffraction and modelling structure files, are included within the
580 supplementary material.

581

582 **Funding**

583 HC would like to thank the UK Medical Research Council (Grant number U105960399)
584 for their support and award of a Career Development Fellowship at MRC-HNR. RJ and
585 JJP would like to also acknowledge the MRC for support (Grant number
586 MR/R005699/1).

587

588 **Competing Financial Interests**

589 None of the authors have any competing financial interests with the work presented
590 here in this manuscript.

591

592 **References**

593 **1.** Bowen H.J.M. & Peggs A. Determination of the Silicon Content of Food. *J. Sci. Food*
594 *Agric.* **35,** 1225-1229 (1984).

595 **2.** Pennington J.A.T. Silicon in foods and diets. *Food Addit. Contam.* **8,** 97-118 (1991).

596 **3.** Iler, R. K. *The Chemistry of Silica*, Wiley, New York, (1979).

597 **4.** Reffitt D.M., Jugdaohsingh R., Thompson R.P.H. & Powell J. J. Silicic acid: its
598 gastrointestinal uptake and urinary excretion in man and effects on aluminium
599 excretion. *J. Inorg. Biochem.* **76,** 141-147 (1999).

600 **5.** Sripanyakorn S., Jugdaohsingh R., Dissayabutr W., Anderson S.H.C., Thompson R.P.T.,
601 & Powell J.J. The comparative absorption of silicon from different foods and food
602 supplements. *Br. J. Nutr.* **102,** 825–834 (2009).

603 **6.** Schwarz K. & Milne, D.B. Growth-promoting Effects of Silicon in Rats. *Nature.* **239,**
604 333-334 (1972).

605 **7.** Carlisle E.M. Silicon: An Essential Element for the Chick. *Science*. **178,** 619-621(1972).

606 **8.** Jugdaohsingh R. *et al.* Increased longitudinal growth in rats on a silicon-depleted diet.
607 *Bone*. **43,** 596-606 (2008).

608 **9.** Garneau, A.P. *et al.* Aquaporins Mediate Silicon Transport in Humans. *PLoS One*, **10**
609 (8)**,** 1-15 (2015).
610
611 **10.** Ratcliffe, S. *et al.* Identification of a Mammalian Silicon Transporter. *Amer. J. Physiol.*
612 *Cell Physiol.* doi: 10.1152/ajpcell.00219.2015 (2017).

613 **11.** Jugdaohsingh, R., Pedro L.D., Watson A. & Powell J.J. Silicon and boron differ in their
614 localization and loading in bone. *Bone Rep.* **1,** 9-15 (2015).

615 **12.** Jugdaohsingh, R., Tucker, K.L., Qiao, N., Cupples, L.A., Kiel, D.P. & Powell, J.J. Silicon
616 intake is a major dietary determinant of bone mineral density in men and pre-
617 menopausal women of the Framingham Offspring Cohort. *J. Bone Min. Res.* **19,** 297–307
618 (2004).
619
620 **13.** MacDonald, H.M., Hardcastle, A.E., Jugdaohsingh, R., Reid D.M. & Powell, J.J. Dietary
621 silicon intake is associated with bone mineral density in premenopausal women and
622 postmenopausal women taking HRT. *J. Bone Min. Res.* **29,** S393 (2005).

623 **14.** Jugdaohsingh, R., Watson, A.I.E., Bhattacharya, P., van Lenthe, G.H. & Powell, J.J.
624 Positive association between serum silicon levels and bone mineral density in female
625 rats following oral silicon supplementation with monomethylsilanetriol. *Osteoporos. Int.*
626 **26,** 1405-1415 (2015).

627 **15.** Hench, L.L., Splinter, R.J., Allen, W.C. & Greenlee, T.K. Bonding mechanisms at the
628 interface of ceramic prosthetic materials. *J. Biomed. Mater. Res. Symp.* **334,** 117-41
629 (1971).

630 **16.** Hench, L.L., Roki, N. & Fenn, M.B. Bioactive glasses: Importance of structure and
631 properties in bone regeneration. *J. Mol. Struct.* **1073,** 24-30 (2014).

632 **17.** Jones, J. R. Review of bioactive glass: From Hench to hybrids. *Acta. Biomater.* **9,**
633 4457-4486 (2013).

634 **18.** Pietak, A.M., Reid, J.W., Stott, M.J. & Sayer, M. Silicon substitituion in the calcium
635 phosphate bioceramics. *Biomater.* **28,** 4023-4032 (2007).

636 **19.** Thian, E.S., Huang, J., Vickers, M.E., Best, S.M., Barber, Z.H. & Bonfield, W. Silicon-
637 substituted hydroxyapatite (SiHA): A novel calcium phosphate coating for biomedical
638 applications. *J. Mater. Sci.* **41,** 709-717 (2006).

639 **20.** Dorozhkin, S. V. Bioceramics of calcium orthophosphates. *Biomater.* **31,** 1465-1485
640 (2010).

641 **21.** Elliott, J. C. *Structure and Chemistry of the Apatites and Other Calcium*
642 *Orthophosphates.* (Elsevier, Amsterdam, 1994) .

643 **22.** Hing K.A., Revell P.A., Smith N. & Buckland T. Effect of silicon level on rate, quality
644 and progerssion of bone healing within silicate-substituted porous hydroxyapatite
645 scaffolds. *Biomater.* **27,** 5014-5026 (2006).

646 **23.** Porter A.E., Patel N., Skepper J.N., Best S.M. & Bonfield W. Effect of sintered silicate-
647 substituted hydroxyaptite on remodelling processes at the bone-implant interface.
648 *Biomater.* **25,** 3303-3314 (2004).

649 **24.** Cameron K., Travers P., Chander C., Buckland T., Campion C. & Noble B. Directed
650 osteogenic differentiaion of human mesenchymal stem/presursor cells on silicate
651 substituted calcium phosphate. *J. Biomed. Mater. Res. A.* **101A,** 13-22 (2013).

652 **25.** Tomoaia, G. *et al.* Silicon effect on the composition and structure of nanocalcium
653 phosphates, in vitro biocompatibility to human osteoblasts. *Mater. Sci. Eng. C.* **37,** 37-47
654 (2014).

655 **26.** Matsunga, K., Murata, H. & Shitara, K. Theoretical calculations of the thermodynamic
656 stability of ionic substitutions in hydroxyapatite under an aqueous solution
657 environment. *J. Phys. Condens. Matter.* **22,** 384210 (2010).

658 **27.** Matsunga, K., Murata, H., Mizoguchi, T. & Nakahira, A. Mechanism of incorporation of
659 zinc into hydroxyapatite. *Acta Biomater.* **6,** 2289-2293 (2010).

660 **28.** Terra, J., Jiang, M & Ellis, D. Characterization of electronic structure and bonding in
661 hydroxyapatite: Zn substitution for Ca. *Phil. Mag.* **82,** 2357-2377 (2002).

662 **29.** Ma, X. & Ellis, D. E. Initial stages of hydration and Zn substitution/occupation on
663 hydroxyapatite (0001) surfaces. *Biomater.* **29,** 257-263 (2008).

30. Tang, Y., Chappell, H. F., Dove, M.T., Reeder, R. J. & Lee, Y.J. Zinc Incorporation into hydroxylapatite. *Biomat.* **30,** 2864-2872 (2009).

31. De Leeuw, N.H. Computer simulations of structures and properties of the biomaterials hydroxyapatite. *J. Mater. Chem.* **20,** 5376-5389 (2010).

32. Astala, R., Calderín, L., Yin, X. & Stott, M. J. Ab Initio Simulation of Si-Doped Hydroxyapatite. *Chem. Mater.* **18,** 413-422 (2006).

33. Friederichs, R.J., Chappell, H.F., Shepherd, D.V. & Best, S. M. Synthesis, characterization and modelling of zinc and silicate co-substituted hydroxyapatite. *Interface,* **12,** 20150190 (2015).

34. Vallet-Regi, M. & Arcos, D. Silicon substituted hydroxyapatite. A method to upgrade calcium phosphate based implants. *J. Mater. Chem.* **15,** 1509-1516 (2005).

35. Leventouri, Th., Bunaciu, C. E. & Perdikatsis, B. V. Neutron powder diffraction studies of silicon-substituted hydroxyapatite. *Biomater.* **24,** 4205-4211(2003).

36. Gibson, I. R., Best, S. M. Best & Bonfield, W. Chemical Characterization of silicon-substituted hydroxyapatite. *Journal of Biomedical Materials Research*, **44** (4), 422-428 (1999).

37. Duncan, J. *et al.* Furthering the understanding of silicate-substitution in α-tricalcium phosphate: An X-ray diffraction, X-ray fluorescence and solid-state nuclear magnetic resonance study. *Acta. Biomater.* **10,** 1443-1450 (2014).

38. Gomes, S. *et al.* Thorough analysis of silicon substitution in biphasic calcium phosphate bioceramics: A multi-technique study. *Acta. Biomater.* **6,** 3264-3274 (2010).

39. Duncan, J., Hayakawa, S., Osaka, A, MacDonald, J. F., Hanna, J. V., Skakle, J. M. S. & Gibson, I. R. Furthering the understanding of silicate-substitution in alpha-tricalcium phosphate: An X-ray diffraction, X-ray fluorescence and solid-state nuclear magnetic resonance study. *Acta Biomaterialia,* **10**, 1443-1450 (2014).

40. Juroszek, R., Czaja, M., Lisiecki, R., Krüger, B., Hachula, B. & Galuskina, I. Spectroscopic and structural investigations of blue afwillite from Ma'ale Adummim

692 locality, Palestinian Autonomy. *Spectrochimica Acta Part A: Molecular and Biomolecular*
693 *Spectroscopy,* **227**, 117688 (2020).

694 **41.** Mehard, C. W & Volcani, B. E. Similarity in Uptkae and Retention of Trace Amounts of
695 ^{31}Silicon and ^{68}Germanium in Rat Tissues and Cell Organelles. *Bioinorganic. Chem.* **5,**
696 107-124 (1975).

697 **42.** Marron, A. O., Chappell, H., Ratcliffe, S. & Goldstein, R. E. A model for the effects of
698 germanium on silica biomineralization in choanoflagellates. *Interface.* **13,** 20160485
699 (2016).

700 **43.** Knight, M. J., Senior, L., Nancolas, B., Ratcliffe, S. & Curnow. P. Direct evidence of the
701 molecular basis for biological silicon transport. *Nature Comms.* **7,** 11926 (2016).

702 **44.** Davies, E. *et al.* Citrate Bridges between mineral platelets in bone. *PNAS.* **111** (14)**,**
703 E1354-E1363 (2014).

704 **45.** Glimcher M.J. Bone: Nature of the Calcium Phosphate Crystals and Cellular,
705 Structural, and Physical Chemical Mechanisms in Their Formation. *Rev. Mineral. Geo.* **64,**
706 223-282 (2006).

707 **46.** Biltz, R. M. & Pellegrino, E.D. The nature of bone carbonate. *Clin. Orthop. Relat. Res.*
708 **129**, 279-292 (1977).

709 **47.** Agna, J. W., Knowles, H. C. & Alverson, G. The Mineral Content of Normal Human
710 Bone. *J. Clin. Invest.* **37** (10), 1357-1361 (1958).

711 **48.** Chappell, H. F., Duer, M. J., Groom, N., Pickard, C. & Bristowe, P.D. Probing the surface
712 structure of hydroxyapatite using NMR spectroscopy and first principles calculations. Phys.
713 Chem. Chem. Phys. **10**, 600-606 (2007).

714 **49.** de Leeuw, N. H. Local ordering of hydroxy groups in hydroxyapatite. *Chem. Comm.*
715 1646 – 1647 (2001).

716 **50.** de Leeuw, N.H. Density functional theory calculations of local ordering of hydroxy
717 groups and fluoride ions in hydroxyapatite. *Phys. Chem. Chem. Phys.* **4,** 3865 – 3878
718 (2002).

51. Suetsugu, Y. & Tanaka, J. Crystal growth and structure analysis of twin-free monoclinic hydroxyapatite. *J. Mater. Sci.: Mater. Med.* **13,** 767-772 (2002).

52. Clark, S. J. *et al.* First principles methods using CASTEP. *Zeitschrift für Krist.* **220,** 567–570 (2005).

53. Monkhorst, H. J. & Pack, J. D. Special points for Brillouin-zone integrations. *Phys. Rev. B.* **13,** 5188–5192 (1976).

54. Vanderbilt, D. Soft self-consistent pseudopotentials in a generalized eigenvalue formalism. *Phys. Rev. B.* **41,** 7892–7895 (1990).

55. Payne, M. C., Arias, T. A. & Joannopoulos, J. D. Iterative minimization techniques for ab initio total-energy calculations: molecular dynamics and conjugate gradients. *Rev. Mod. Phys.* **64,** 1045–1097 (1992).

56. Posner, A. S. Crystal Chemistry of bone mineral. *Physiol. Rev.* **49,** 760-792 (1969).

57. Chappell H.F. & Bristowe P.D. Density functional calculations or the properties of silicon-substituted hydroxyapatite. *J. Mater. Sci.: Mater. Med.* **18,** 829-837 (2007).

58. Jugdaohsingh, R., Watson, A.I.E., Pedro, L.D. & Powel, J.J. The decrease in silicon concentration of the connective tissueswith age inrats is a marker of connective tissue turnover. *Bone*. **75,** 40-48 (2015).

59. Kim, H.M., Rey, C. & Glimcher, M.J. Isolation of calcium-phosphate crystals of bone by non-aqueous methods at low temperature. *J. Bone Miner. Res.* **10,** 1589-1601 (1995).

60. Generated using CrystalDiffract®: a powder diffraction program for Mac and Windows. CrystalMaker Software Ltd, Oxford, England (www.crystalmaker.com)

61. Carlisle E.M. Silicon: A Possible Factor in Bone Calcification. *Science.* **167,** 279-280 (1970).

62. Landis W.J., Lee D.D., Brenna J.T., Chandra S. & Morrison G.H. Detection and Localization of Silicon and Associated Elements ub Vertebrate Bone Tissue by Imaging Ion Microscopy. *Calcif. Tissue Int.* **38,** 52-59 (1986).

746 **63.** Boonrungisman S. *et al.* Correlative spectroscopy of silicates in mineralised nodules
747 formed from osteoblasts. *Nanoscale* **5,** 7544-7551 (2013).

748 **64.** Chakkalakal, D. A., Mashoof, A. A., Novak, J., Strates, B.S. & McGuire, M. H.
749 Mineralization and pH relationships in healing skeletal defects grafted with
750 demineralized bone matrix. *J. Biomed. Mater. Res.* **28,** 1439-1443 (1994).

751 **65.** Kaysinger, K. K. & Ramp, W. K. Extracellular pH Modulates the Activity of Cultured
752 Human Osteoblasts. *J. Cell. Biochem.* **68,** 83-89 (1998).

753 **66.** Iler, R. K. The Chemistry of Silica: Solubility, Polymerisation, Colloid and Surface
754 Properties, and Biochemistry. New York: John Wiley & Sons. 1979

755 **67.** Eisinger, J. & Clairet, D. Effects of silicon, fluoride, etidronate and magnesium on
756 bone mineral density: a retrospective study. *Magnes. Res.* **6,** 247-249 (1993).

757